Determination of normal and inverse magnetocaloric effect in iron oxide thin films

Murtaza Bohra, Prakhar Gupta, Dharohar Sahadot, Anil Annadi, Vidyadhar Singh, Jean-François Bobo

Determination of normal and inverse magnetocaloric effect in iron oxide thin films

Murtaza Bohra[1], Prakhar Gupta[1], Dharohar Sahadot[1], Anil Annadi[1], Vidyadhar Singh[2], Jean-François Bobo[3]*

[1]Mahindra University, Survey Number 62/1A, Bahadurpally, Jeedimetla, Hyderabad–500043, Telangana, India

[2]Department of Physics, Jai Prakash University, Chapra, Bihar 841301, India

[3]Centre d'Elaboration de Materiaux et d'Etudes Structurales (CEMES), 29 rue Jeanne Marvig, 31055 Toulouse Cedex 4, France

Abstract

Magnetic cooling requires energy-efficient and eco-friendly alternatives to conventional rare earth element-based materials, which rely on materials with customized magnetic and structural properties. This study introduces the growth of iron oxide thin films for designing magnetocaloric materials, using a phenomenological model to screen candidates for the magnetocaloric effect (MCE) and inverse magnetocaloric effect (IMCE). Based on the Curie temperature (T_C) window concept, ferrimagnetic Fe_3O_4 and the antiferromagnetic α–Fe_2O_3 and FeO thin films are identified as potential candidates for structural transitions (T_V) and spin rearrangement (T_N) achieved by manipulating their nanoscale ordering temperatures. These oxide films exhibit IMCE with a maximum entropy change (ΔS_{max}) ranging from 0.13 to 1.87 J/kg-K at T_V and/or T_N, while demonstrating the MCE effect at low temperatures. Interestingly, we demonstrate that IMCE can occur in Fe_3O_4 thin films without a structural transition but with a change in anisotropy. Additionally, utilizing textured growth to tailor magneto-structural coupling in thin films is predicted as a novel approach for engineering magnetocaloric materials.

Keywords: *Magnetocaloric effect and inverse magnetocaloric effect, Iron oxide thin films, Verwey transition, Magnetic cooling, Antiferromagnetic transition*

***Corresponding author**: murtaza.bohra@mahindrauniversity.edu.in*

Introduction

Manipulating the crystalline phases of magnetic materials provides an enticing opportunity for designing magnetic cooling devices, as it enables the control of both the normal Magnetocaloric Effect (MCE) and the Inverse Magnetocaloric Effect (IMCE) [1-3].The MCE in terms of entropy change (ΔS) comprises three main contributions: $\Delta S = \Delta S_L + \Delta S_E + \Delta S_M$. These contributions stem from changes in magnetic entropy (ΔS_M), lattice entropy (ΔS_L), and electronic entropy (ΔS_E) [4]. The ΔS_M is a function of both *H* and *T*, but ΔS_L and ΔS_E are functions of *T* only hence ΔS_M have dominant contributions when changing the strength of *H*. Normally, strong MCE occurs upon exposure of a magnetic material to external magnetic fields near its magnetic phase transitions (Curie temperature, T_C) of the ferrimagnetic (FIM) material. However, IMCE effects have been observed near the antiferromagnetic (AFM) transition temperature (Neel temperature, T_N) [5-9], as well as the spin glass (SG) transition temperature (T_G) [1-2]. In some materials, the coexistence of both MCE and IMCE behaviors has been observed, with IMCE being observed at far lower temperatures compared to the MCE [5-9]. Recent findings indicate that IMCE can manifest without the requirement of AFM/SG interactions. Instead, a mere increase in magnetic anisotropy proves to be adequate [5]. Consequently, it is recommended to explore different types of strongly correlated magnetic materials that exhibit simultaneous spin, charge, and lattice coupling, resulting in MCE and IMCE over various temperature ranges, which are desirable for efficient magnetic refrigeration devices.

By employing oxidation/reduction approaches, various forms of iron oxides can be stabilized in a reversible manner (see scheme 1), leading to structural transformations that, in turn, affect magnetic anisotropy [10-15]. The iron oxide consists of many technologically important compounds like AFM (FeO; T_N=*198 K* and α–Fe_2O_3; T_N=*940 K*) and FIM (γ–Fe_2O_3; T_C=*833 K* and Fe_3O_4; T_C= *858 K*) phases [10-15] with distinct correlated electric and magnetic properties (see scheme 1). On top of this, the Fe_3O_4 and α–Fe_2O_3 compounds exhibit temperature-driven Verwey transition (T_V=*120 K*) and Morin transitions (T_M=*260 K*), respectively, where the former is accompanied by a structural transition [16] and the latter by an inversion of planar spin arrangement [5]. The α–Fe_2O_3 displays AFM order below T_M and weak FM order above T_M, while Fe_3O_4 remains FIM across T_V. However, it has been reported that these transitions shift to lower temperatures with decreasing nanoparticle sizes and tend to vanish below critical sizes [17]. The MCE, expressed as $\Delta T = -\frac{T}{C_P}\left(\frac{dM}{dT}\right)_H \Delta H$, for aqueous suspensions of super fine iron oxide particles (α–Fe_2O_3, γ–Fe_2O_3, and Fe_3O_4) at finite field change and adiabatic conditions, exhibited a positive magnitude for all investigated systems except the α–Fe_2O_3 system [18]. However, this estimation was only conducted around room temperature; no study has been reported around T_M and T_V. While numerous spinel ferrites have been identified as magnetic refrigerants [19-20], the search continues for

thin-film ferrite materials showcasing significant MCE and substantial relative cooling power (RCP). Previously, we have studied various anomalous magnetic properties of nanocrystalline Fe_3O_4 thin films [21] compared to other ferrite nanomaterials [22-26], but detailed MCE data of various iron oxide thin films are still lacking. In the present study, we simulated the MCE and IMCE across different magnetic transitions in terms of entropy change, ΔS in iron oxide thin films using a phenomenological model. This approach not only enhances the potential for designing MCE materials with a broader temperature range but also substantiates the universality of this concept.

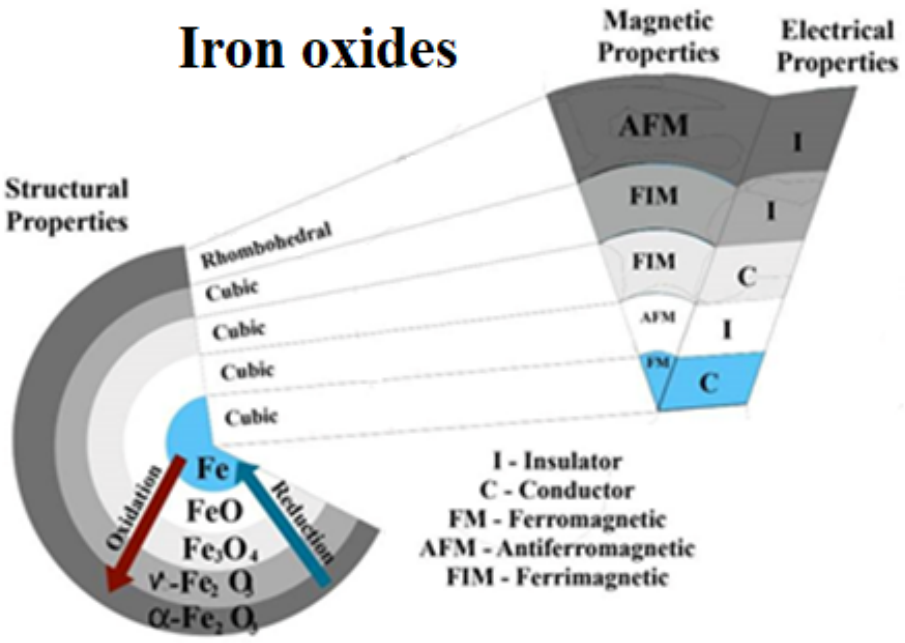

Scheme 1. Various technological important iron oxide materials

Experimental details

Iron oxide films were grown on amorphous fused quartz substrate by pulsed laser ablation of α–Fe_2O_3 target at various growth temperatures, T_S = room temperature (RT)–850 °C [27]. Deposition was carried out in vacuum of 1×10^{-5} mbar with laser energy density of 2.5 J/cm^2. Few films were later annealed in hydrogen atmosphere at 450 °C for 15 minutes to get Fe_3O_4 phase. X-ray diffraction (XRD) was taken by a PANalytical X'Pert PRO X-ray diffractometer using CuK_α radiation. Phase purity of the film was also confirmed by micro-Raman spectroscopy, which is very sensitive to different phases of iron oxides. The

micro-Raman spectra were recorded in the range of 100–1000 cm^{-1} with a 6 mW, 514.5 nm Ar^{+} laser source. Magnetization as a function of temperature (*M–T*) was measured with in plane film configuration by using a Quantum design PPMS in a fixed magnetic field.

Results and discussion

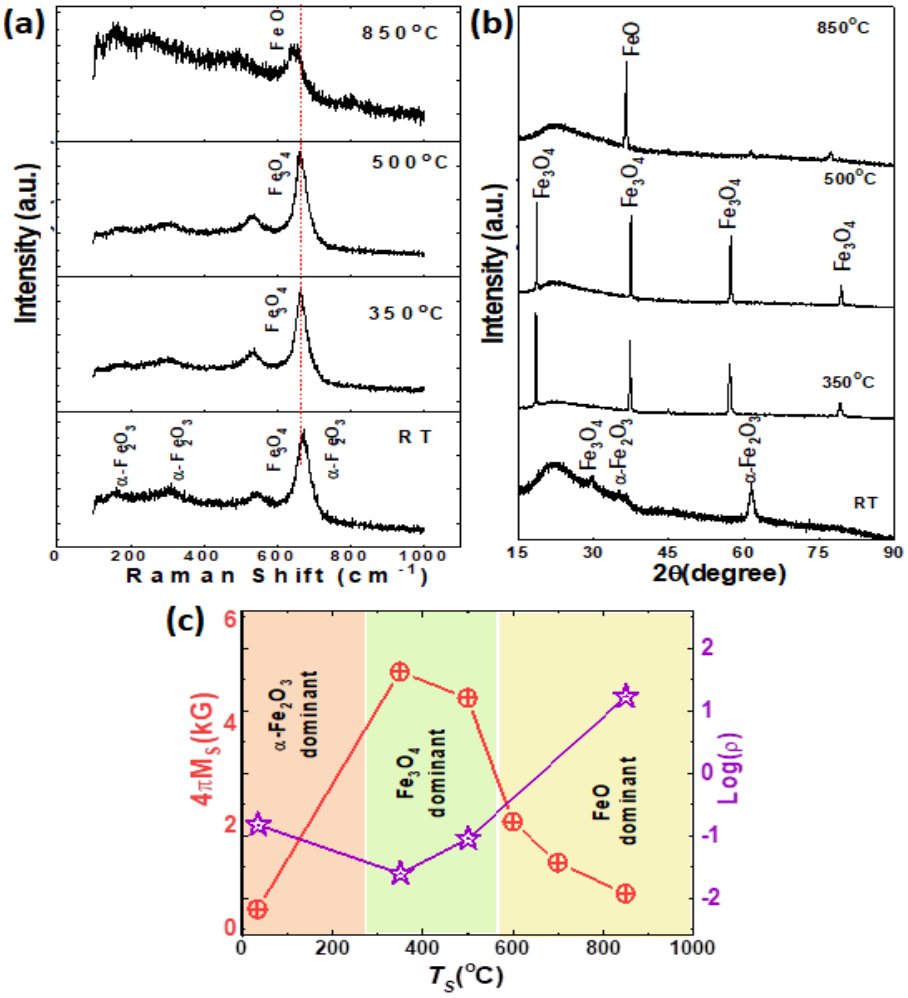

Figure 1. Raman spectra (a) and XRD [27] patterns (b) for T_S= RT– 850 °C iron oxide thin films. Room temperature saturation magnetization ($4\pi M_S$) and resistivity (ρ) values with T_S.

Detailed structural analysis by Raman spectra (Figure 1(a)) and XRD (Figure 1(b)) suggests that in iron oxide thin films, the dominant phase at low T_S is α–Fe_2O_3, transitioning to Fe_3O_4 in intermediate T_S films,

and ultimately transforming into the FeO dominant phase in the highest T_S films. These findings are further supported by room temperature resistivity (ρ_{300K}) and saturation magnetization (M_S) data (Figure 1(c)), showing higher ρ_{300K} and lower M_S values in α–Fe_2O_3 and FeO containing samples.

We have plotted *M–T* curves of these films in Figure 2 at a fixed field of 0.5 T. The T_S of the RT films shows a Morin transition occurring around T_M = 60 K, which is expected to take place in bulk α-Fe_2O_3 at 260 K [10]. This discrepancy could be attributed to the lower grain sizes (~12-14 nm) in the films. In the T_S of the 350 °C films, a broad Verwey transition of Fe_3O_4 occurs at T_V =120 K, which becomes even sharper in the T_S of the 500 °C films. However, in the T_S of the 850 °C films, an AFM transition of FeO appears, overlapping with the Verwey transition of residual Fe_3O_4. The zero coercivity value and high non-saturation magnetization in low temperature *M-H* loops (Supplementary information Fig. S1) confirms the Morin transition and Neel transitions of AFM α–Fe_2O_3 and FeO phases, respectively, while the enhanced coercivity value confirms the Verwey transition in the monoclinic phase of FIM Fe_3O_4 [27].

We have fitted these *M–T* curves using modified phenomenological model. This model precisely describes the magnetization behavior in two parts while FM part was fitted with Bloch type law [27] in region-I:

$$M = M_0\left[1-\left(\frac{T}{T_C}\right)^n\right] \qquad (1)$$

where M_0 is the saturation magnetization at 0 K, and n is the Bloch exponent. Below AFM and Verwey transition where magnetization start falling we have fitted *M–T* curves using inverse Gaussian expression in region II,

$$M = -[M_0 + D\exp\left\{-\frac{\left(T-T_F\right)^2}{2w^2}\right\}] \qquad (2)$$

where T_F is minima of magnetization and D and w are fitting parameters. A reasonably good simulated *M–T* curves can be generated from equation (1) and (2) for all samples as shown in the Insets of Figure 2. By using approximated T_C and T_F values and other fitting parameters given in Table 1, we can simulate the MCE in terms of magnetic entropy change, ΔS of our samples at fixed field of H_{max}= 0.5 T. The ΔS can be formulated using the Maxwell relation: $\Delta S = \int_0^{H_{max}} \left(\frac{\partial M}{\partial T}\right)_H dH$ [4]. In FM region-I , ΔS can be expressed as:

$$\Delta S = -\frac{nT^{n-1}}{T_c^{\,n}} M_0 H_{max} \qquad (3)$$

In region-II, one needs to use expression:

$$S = H_{max} E(T - T_F) \exp[-\frac{(T - T_F)^2}{2w^2}] \qquad (4)$$

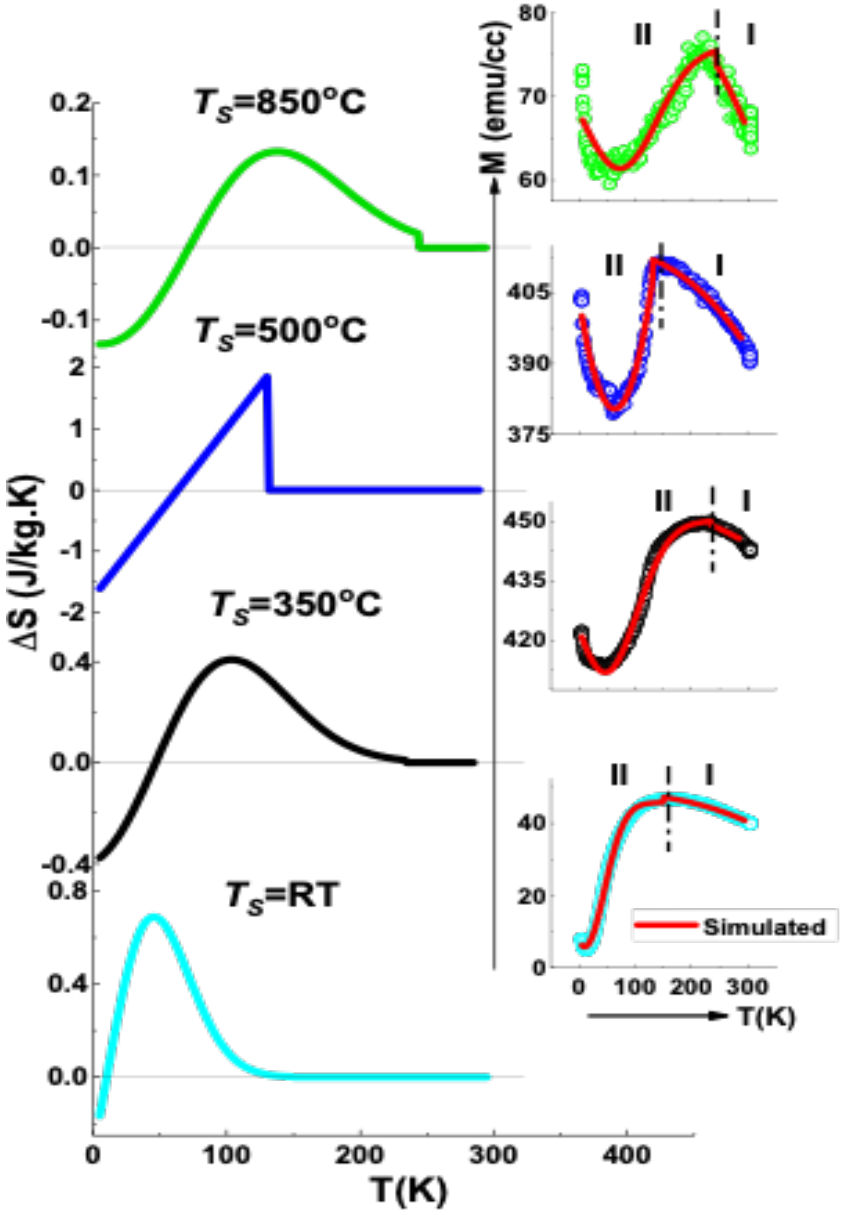

Figure 2. Simulated ΔS–T curves for different T_S films. Insets show corresponding experimental [27] and simulated M–T curves at fixed field of 0.5 T.

Table 1. *Simulated parameters of M–T curves (T_F, T_C and n) and ΔS–T curves (ΔS_{max} and RCP) for different T_S films at fixed filed of 0.5 T.*

Fit parameters	T_S =RT	T_S =350 °C	T_S =500 °C	T_S =850 °C
T_F (K)	10.15	46.70	63.204	71.71
n	2.5	2.5	2.5	2.5
T_C (K)	608.68	1367	983.25	545.48
ΔS_{max} (J/kg-K)	0.67	0.41	1.87	0.13
RCP (J/kg)	30.94	37.03	52.77	10.59

Figure 2 shows the simulated ΔS–T curves for all samples and corresponding fitting parameters are given in Table 1. The IMCE in terms of maximum value of ΔS_{max} can be observed in all samples at their T_V and T_N values ranging from 0.13 − 1.87 J/kg-K at fixed filed of 0.5 T. Interestingly, all samples exhibit a coexistence of IMCE and MCE behavior, where ΔS transitions from positive to negative values at low temperatures around their respective T_F values. Similar IMCE effect have been observed in $ZnFe_2O_4$ layers below T_N of 15 K due to contribution from AFM grains [28], as well as in the bulk $Y_2Ir_{2-x}Cr_xO_7$ compounds below their cluster glass transition temperatures, T_G of 15 – 35 K [1]. The magnetization decreases with temperature below T_F, resulting in a negative dM/dT and a sign conversion of the ΔS–T curves. The ΔS_{max} is reduced in the T_S of the 850 °C films due to lower magnetization values. The broadening of ΔS peaks, other than the T_S of the 500 °C film, can be attributed to multiple iron oxide phases creating different ΔS values near their magnetic transitions across a wide temperature range. Thus, iron oxide layers grown at different T_S may be operated in magnetic refrigeration that uses magnetization and demagnetization processes to exploit both positive and negative magnetic entropy variations. Although our observed values of the MCE and IMCE are not large, they are comparable to those reported for many materials, such as $La_{0.7}Sr_{0.3}MnO_3$ [8] and Fe_3O_4 [29] thin film [8], $SmCaCoMnO_6$(94%) and $SmMnO_3$(6%) nanocomposites [2], as well as bulk pyrochlore oxides and other Ir-based systems [1]. The

effect of large working temperature window may lead to the enhancement of relative cooling power, *RCP* = $|\Delta S_{max}| \times \Delta T_{FWHM}$ [1]. The *RCP* measures the amount of heat transferred between the hot and cold reservoirs in one refrigeration cycle, which is estimated to be in the range of 10.59 – 52.77 J/kg in ours samples at fixed filed of 0.5 T.

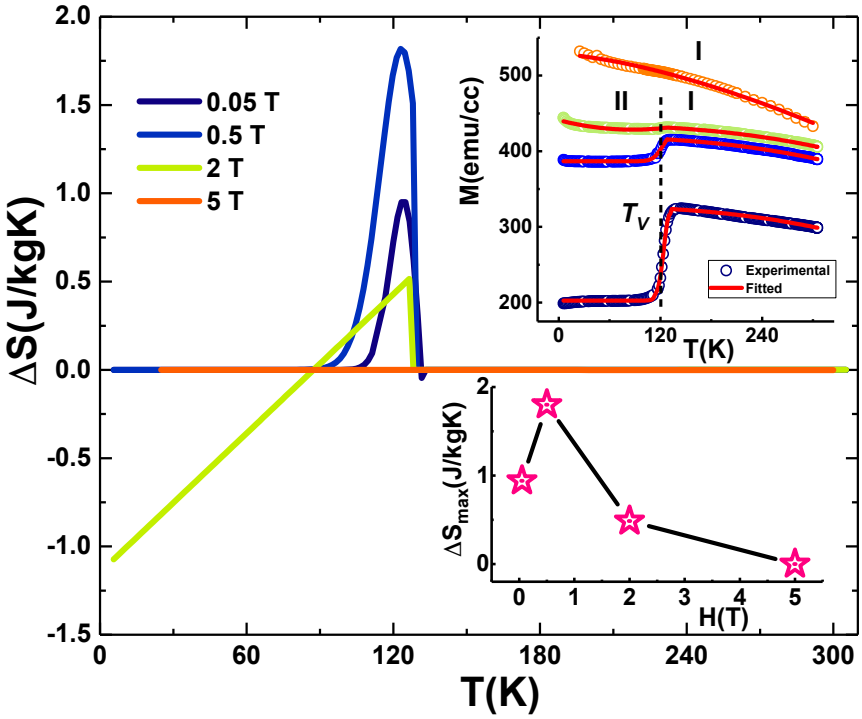

Figure 3. Simulated ΔS–T curves for different applied field for T_S of the 500 °C Fe_3O_4 films. Top Inset show corresponding experimental [31] and simulated M–T curves for different applied field. Bottom Inset shows ΔS_{max} vs. H curve.

Understanding the impact of structural transitions on IMCE in terms of ΔS is crucial for the design of magnetocaloric materials with high performance. This understanding relies on various factors, including particle size, phase transition temperature, applied magnetic field, and the presence of different magnetic phases [8]. We have chosen T_S of the 500 °C Fe_3O_4 films, which exhibits a sharp Verwey transition within the ferromagnetic state. This transition is typically attributed to a cubic-to-monoclinic structure transformation at T_V = 120 K. The purpose of our study is to investigate the impact of an external magnetic field (H) on the ΔS–T simulated curves, which are depicted in Figure 3. With increasing H from 0.05 to 2 T, the ΔS peak broadens and eventually smears out at 5 T. In the bottom inset of Figure 3, the plotted ΔS_{max} values demonstrate an increasing trend from 0.05 to 0.5 T, followed by a gradual decrease to zero at 5 T. The ΔS_{max} (*RCP*) values were found to be in the range of 0.48 to 1.8 J/kg-K (12.8

to 58.8 J/kg) with increasing field from 0.05 to 5 T (Supplementary information Table S1). Normally, FM systems follow a power law $\Delta S_{max} = aH^n$, where 'a' is a constant and the exponent 'n' is theoretically predicted to be 2 according to the Curie law above T_C [8]. Similar, IMCE was found in bulk $Pr_{0.58}Sr_{0.42}MnO_3$ within the ferromagnetic state at the orthorhombic to monoclinic structural transition, where the ΔS peak showed weak dependence on H [5]. In nanocrystalline manganites, the exponent 'n' reaches 1 for $T \leq T_C$ and 2 for $T \geq T_C$, respectively [30]. To comprehend this unusual IMCE found at T_V in Fe_3O_4 films, we plotted simulated M–T curves measured at different H in the top inset of Figure 3. The magnitude of the magnetization drops (ΔM) at T_V is highly dependent on H, with no observed drop at H = 5 T, and typically follows equation (1). The ΔM occurs because $H < 5$ T is insufficient to fully saturate the magnetization of the anisotropic monoclinic phase. The ΔM raises the question of whether it arises from a change in the magnetic moment of Fe_3O_4 or from increased anisotropy [30]. It can occur without a structural transition, as long as there is a change in anisotropy [22, 30]. The Verwey transition is basically a structural transition in which anisotropy increases in the monoclinic phase of Fe_3O_4 below 120 K. The application of a low field cannot saturate the sample, resulting in a magnetization drop. However, at higher fields, no such effect can be observed. This clearly indicate that the Verwey transition has nothing to do with a change in magnetic interaction but rather involves a change in anisotropy [31-32]. Thus, the observed field-dependent ΔS-T curves suggest that the occurrence of IMCE does not require AFM interactions or structural transitions. Instead, an increase in magnetic anisotropy is sufficient. Additionally, in a ferromagnetic system, the value of the maxima of ΔS_{max} at the Curie temperature usually increases with an increasing magnetic field. However, in the case of the Verwey transition, ΔM reduces with the field, leading to a reduction in ΔS_{max}.

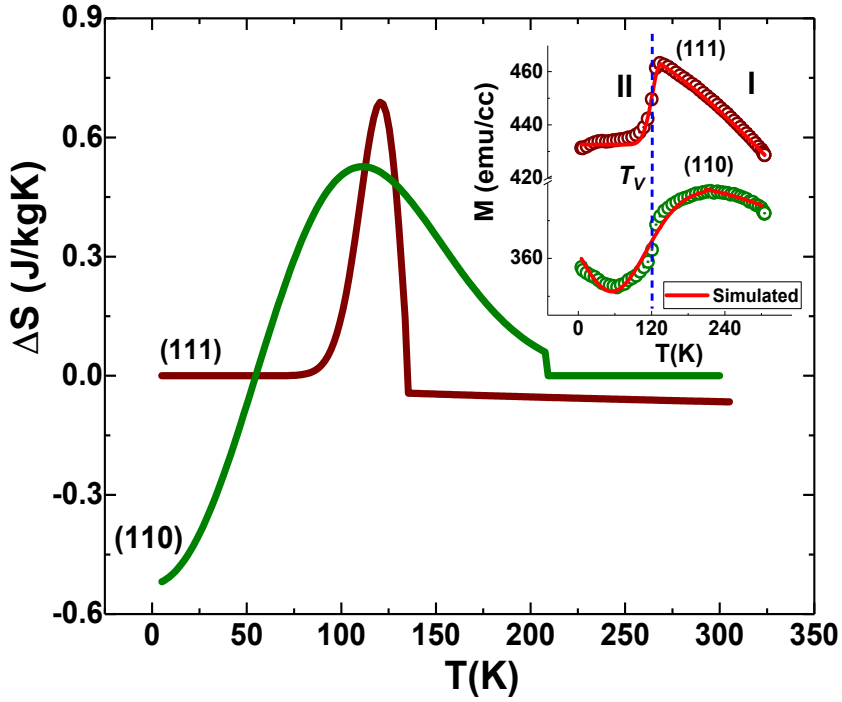

Figure 4. Simulated ΔS–T curves for (111) and (110) textured Fe_3O_4 films. Inset shows corresponding experimental [27] and simulated M–T curves at fixed field of 0.5 T.

We have also investigated how the textured growth of Fe_3O_4 films affects the ΔS–T curves because [111], [110] and [100] represent the easy, intermediate and hard directions of magnetization in the cubic phase of Fe_3O_4 [31]. The (111) and (110) textured growth can be achieved in hydrogen-annealed Fe_3O_4 films with T_S of RT and 350 °C, respectively (Supplementary information, Fig. S2). The substrate is essentially composed of amorphous fused quartz, so no strain is expected to arise from it. However, the growth temperature plays a crucial role in determining textures, especially the (111) plane, which represents the closest packing plane in the cubic system. Most films are grown at temperatures $T_S \geq 200$ °C in a manner that aligns with the (111) plane. The corresponding simulated ΔS–T curves, shown in Figure 4, exhibit a broad ΔS peak in (110) textured films compared to the narrow peak in (111) textured films, with the latter having higher ΔS_{max} (0.7 J/kgK) values at a fixed field of 0.5 T (Supplementary information Table S2). On the other hand, the (110) textured films have three times larger RCP (47.25 J/kg) values than (111) textured films. The reason for this difference can be attributed to their M–T curves (inset of Fig. 4). In the case of (111) textured films, the magnetization increases at a faster rate between 120–300 K, following Bloch's law with n = 3/2. However, for (110) textured films, it is evident that a 0.5 T field is inadequate to fully saturate the magnetization, and they adhere to Bloch's law with n = 5/2. This further affects the broadening of the Verwey transition and low-temperature magnetization behaviors. Below T_V, in the monoclinic phase of Fe_3O_4, [100] now becomes the easy axis compared to [111] [30-32]. This change may be reflected in the increasing magnetization observed in (110)-textured films at low temperatures,

resulting in a changeover of ΔS values from positive to negative. Thus, the textured growth in a specific crystalline direction provides a second lever of action that enables tuning of the MCE properties. By using crystalline substrates, magneto-structural coupling can be further tuned in epitaxial thin films.

Conclusion

In summary, the opportunity to manipulate both MCE and IMCE by inducing structural changes in our iron oxide thin films through T_S offers exciting possibilities, particularly for applications requiring low temperatures. The proposed phenomenological model allows for simulating the magnetic entropy change of an IMCE and MCE material, which is imperative to judge its suitability in advancing magnetic refrigeration technology. The IMCE was observed near the Verwey transition and antiferromagnetic transition temperatures in nanocrystalline Fe_3O_4, α–Fe_2O_3 and FeO thin films, respectively. The maximum magnetic entropy changes, ΔS_{max}, and relative cooling power, RCP, are found to be 0.13 – 1.87 J/kg-K and 10.59 – 52.77 J/kg, respectively, at a fixed field of 0.5 T achievable with a laboratory electromagnet. We demonstrate that the occurrence of these transitions is not a necessary condition for IMCE; instead, an increase in magnetic anisotropy is sufficient. Importantly, our findings indicate that the IMCE is more pronounced in Fe_3O_4 thin films with (111) texture when compared to those with (110) texture.

Acknowledgment: We thank Dr. Shiva Prasad and Dr. N. Venkataramani from IIT Bombay (India) for allowing use of their experimental facilities. We also thank to Dr. S.C. Sahoo from IIT Bombay (India) for assisting with the magnetic measurements.

Author contributions: All authors contributed to the study conception and design. MB, DS, PG, AA, VS and JFB contributed to executing data analysis, writing the manuscript, drawing figures, and manuscript revision. All authors read and approved the final manuscript.

Data availability

All data generated during this study are contained in this published article.

Declarations

Conflict of interest

The authors declare that they have no known competing financial Interests or personal relationships that could have appeared to influence the work reported in this paper.

References

1. Dwivedi V K, Mandal P and Mukhopadhyay S 2022 *ACS Appl. Electron. Mater.* **4** 1611
2. Akram W, Bansal M, Pradeep R P, Kaipamangalath A, Giri S K and Maity T 2023 *Phys. Rev. B* **107** 224403
3. Biswas A, Chandra S, Samanta T, Phan T M, Das I and Srikanth H 2013 *J. Appl. Phys.* **113** 17A902
4. Yu B F, Gao Q, Zhang B, Meng X Z and Chen Z 2003 *Int. J. Refrig.* **26** 622–636
5. Maheswar Repaka D V, Aparnadevi Kumar M P, Tripathi T S and Mahendiran R 2013 *J. Appl. Phys.* **113** 17A906
6. Patra M, Majumdar S, Giri S, Iles G N and Chatterji T 2010 *J. Appl. Phys.* **107** 076101
7. Morozkin A V, Yapaskurt V O, Yao J, Nirmala R, Quezado S and Malik S K 2019 *Intermetallics* **107** 81–92
8. Mottaghi N, Trappen R B, Sarraf S Y, Seehra M S and Holcomb M B 2020 *J. Alloys Compd.* **826** 154200
9. Giri S K, Dasgupta P, Poddar A and Nath T K 2015 *J. Alloys Compd.* **631** 266
10. Jani H, Linghu J, Hooda S, Chopdekar R V, Li C, Omar G J, Prakash S, Du Y, Yang P, Banas A, Banas K, Ghosh S, Ojha S, Umapathy G R, Kanjilal D, Ariando A, Pennycook S J, Arenholz E, Radaelli P G, Coey J M D, Feng Y P and Venkatesan T 2021 *Nat. Commun.* **12** 1668
11. Bohra M 2022 *J. Electron. Mater.* **51** 2709–2715
12. Tong S, Quinto C A, Zhang L, Mohindra P and Bao G 2017 *ACS Nano* **11** 6808
13. Sinmyo R, Bykova E, Ovsyannikov S V, McCammon C, Kupenko I, Ismailova L and Dubrovinsky L 2016 *Sci. Rep.* **6** 32852
14. Namai A, Yoshikiyo M, Yamada K, Sakurai S, Goto T, Yoshida T, Miyazaki T, Nakajima M, Suemoto T, Tokoro H and Ohkoshi S I 2012 *Nat. Commun.* **3** 1035
15. Sakurai S, Namai A, Hashimoto K and Ohkoshi S 2009 *J. Am. Chem. Soc.* **131** 18299

    Ukleev V, Suturin S, Nakajima T, Arima T H, Saerbeck T, Hanashima T, Sitnikova A, Kirilenko D, Yakovlev N and Sokolov N 2018 *Sci. Rep.* **8** 8741
16. Bohra M, Agarwal N and Singh V 2019 *J. Nanomater.* 1–8
17. H. M. Lu and X. K. Meng, 2010 *J. Phys. Chem. C*, **114**, 49, 21291

18. V. V. Korolev, I. M. Arefyev and A. G. Ramazanova, 2008 *Journal of Thermal Analysis and alorimetry*, **92**, 3, 691.
19. Poddar P., Gass J., Rebar D. J., Srinath S., Srikanth H., Morrison S. A., Carpenter E. E., 2006 Journal of Magnetism and Magnetic Materials. 307 227.
20. Chau N., Thuan N., Minh D., Luong N., 2008 Journal of Science Mathematics -Physics. **24** 155.
21. Bohra M, Roy Chowdhury D, Bobo J F and Singh V 2019 *J. Appl. Phys.* **125** 013901
22. M. A. Almessiere, Y. Slimani, A. Demir Korkmaz, A. Baykal, H. Güngüneş, H. Sözeri, Sagar E. Shirsath, S. Güner, S. Akhtar, A. Manikandani, 2019 *RSC Adv.* **9,** 30671.
23. Y. Slimani, B. Unal, M. A. Almessiere, A. Demir Korkmaz, Sagar,E. Shirsath, Ghulam Yasin, A.V. Trukhanov, A. Baykal, 2020 *Results in Physics* **17**, 103061.
24. M. Abdullah Almessiere, Y. Slimani, H. Güngüneş, S. Ali, A. Manikandan, I. Ercan, A. Baykal, A.V. Trukhanov, 2019 *Nanomaterials*, **9** 820.
25. P. Annie Vinosha, A. Manikandan, A. Sherley Judith Ceicilia, A. Dinesh, G. Francisco Nirmala, A. Christy Preetha, Y. Slimani, M.A. Almessiere, A. Baykal, Belina Xavier, 2021 *Ceramics International*, **47**, 10512.
26. M. A. Almessiere, Y. Slimani, S. Güner, A. Baykal, I. Ercan, 2019 *Journal of Rare Earths*, **37**, 871.
27. Bohra M, Prasad K E, Bollina R, Sahoo S C and Kumar N 2016 *J. Magn. Magn. Mater.* **418** 137
28. Bohra M, Singh N, Annadi A, Vittal S and Singh V 2023 *Mater. Res. Bull.* (under review)
29. Bohra M and Sahoo S C 2017 *J. Alloys Compd.* **699** 1118–1121
30. Pekala M 2010 *J. Appl. Phys.***108** 113913
31. Bohra M, Prasad S, Venketaramani N, Kumar N, Sahoo S C, R. Krishnan R 2009 *J. Magn. Magn. Mater.* **321** 3738–3741
32. Kąkol Z, Król G, Tabiś W, Kołodziej T, Wiśniewski A, Stepankova H, Chlan V, Kusz J, Tarnawski Z, Kozłowski A and Honig J M 2011 *J. Phys.: Conf. Ser.* **303** 012106